Journal of Magnetic Resonance 220 (2012) 45–53

Contents lists available at SciVerse ScienceDirect

Journal of Magnetic Resonance

journal homepage: www.elsevier.com/locate/jmr

Spectral spatial electron paramagnetic resonance imaging as a tool to study photoactive dimethacrylate-based dental resins

Philippe Levêque [a,b], Julian G. Leprince [b,c,d,1], Sabine Bebelman [c], Jacques Devaux [b,c], Gaëtane Leloup [b,c,d], Bernard Gallez [a,b,*]

[a] Biomedical Magnetic Resonance Research Group, Louvain Drug Research Institute, Université catholique de Louvain, Brussels, Belgium
[b] Center for Research and Engineering on Biomaterials CRIBIO, Université catholique de Louvain, Brussels, Belgium
[c] Institute of Condensed Matter and Nanosciences, Bio- and Soft-Matter, Université catholique de Louvain, Louvain-la-Neuve, Belgium
[d] School of Dentistry and Stomatology, Université catholique de Louvain, Brussels, Belgium

ARTICLE INFO

Article history:
Received 27 January 2012
Revised 20 April 2012
Available online 1 May 2012

Keywords:
EPR
Imaging
Dental resin
Free radicals
Dimethacrylate
Biomaterials

ABSTRACT

Photopolymerizable dimethacrylate-based dental resins, which are widely used in the current routine dental practice, show a very strong EPR signal. This signal has already been studied by EPR spectroscopy, but not by EPR imaging. The spectrum is quite complex due to hyperfine splitting and to the presence of two radical species, which is a priori not favorable to EPR imaging.

In this work, the robustness of EPR imaging was investigated, both in the spatial and spectral-spatial modes, to characterize this type of material using small resin samples. The images produced using standard deconvolution and filtered backprojection procedure did not display any noticeable artifact. They also reflected the expected density of free radicals in two types of resin, photopolymerized with two different light irradiances.

Moreover, the spectral-spatial imaging mode provided a complete spectrum for each pixel, which enabled to delineate the different distributions of the two radical species inside the samples. EPR imaging offered a different information compared to the usual degree of conversion measured by Raman spectrometry. These results suggest that EPR imaging could be used as a complementary tool to further characterize the dimethacrylate-based resins used in dental practice or for other applications.

1. Introduction

Electron Paramagnetic Resonance (EPR) spectroscopy is a sensitive method used to detect paramagnetic centers, such as unpaired electrons or free radicals, in a large variety of applications [1–3]. Because it is a spectroscopic method, it lacks spatial information and gives a signal which is the summation of all the contributions of the paramagnetic centers in the measured volume.

EPR spatial information can be obtained if magnetic field gradients are used, similarly to NMR imaging. The linear gradient of field is produced by an additional set of coils and induces a variation of the resonance condition along the direction of the gradient, allowing spatial encoding. Because the linewidth of the EPR signal is a few orders of magnitude larger than NMR signal, stronger gradient of field must be used [4].

Although EPR Imaging (EPRI) has been used for several decades now [5], commercially available equipments are relatively recent and the technique is still in the beginning of a growing use. After its initial use in the field of material sciences studying paramagnetic centers in materials such as diamonds [6,7], EPRI was extended to *in vivo* applications in the early 1980s [8–11].

EPR images can be acquired using two different modalities, the continuous-wave (CW) approach or the time-domain (also called pulsed or Fourier transformation) approach [12]. In CW-EPR imaging, the frequency is kept constant and the field is swept, whereas in the pulsed approach the field is kept constant and the impulse response of the system is acquired. Although FT-EPR allows a much faster data acquisition than CW-EPRI, it is limited by the very fast relaxation process of electrons, and is in practice restricted to the imaging of probes with a relatively long T2, or a narrow linewidth. Therefore, CW is currently the most widely used modality. During the field sweep, successive so-called isofield planes, orthogonal to the direction of the linear gradient, are brought into resonance and the integral of the projection is recorded. To cover the entirety of the volume of the object in a 2D image, the orientation of the gradient is rotated in the selected plane in equal intervals, following the classical principle of tomographic acquisition.

* Corresponding author at: Biomedical Magnetic Resonance Group, Louvain Drug Research Institute, Avenue Mounier 73 – B1.73.08, 1200 Brussels, Belgium. Fax: +32 2 764 73 90.
E-mail address: Bernard.gallez@uclouvain.be (B. Gallez).
[1] JL is a Postdoctoral Researcher at F.R.S.-FNRS.

1090-7807/$ - see front matter © 2012 Elsevier Inc. All rights reserved.
http://dx.doi.org/10.1016/j.jmr.2012.04.014

The magnitude of the gradient is determined based on the desired resolution, and on the linewidth of the signal of the paramagnetic center. In order to spatially resolve two points separated by a distance d (m), the magnitude of the gradient G (mT/m) should be greater than the ratio of the linewidth LW (mT) of the signal to this distance d according to the following equation [11].

$$G \geqslant LW/d \quad (1)$$

The resolution will increase with the magnitude of the gradient, but a strong gradient will also distort the spectrum to some extent, inducing a broadening of the spectrum and consequently a decrease of the signal intensity and of the signal to noise ratio (SNR) [13]. Spectral information is still present in the projection, so that a deconvolution step is usually applied before reconstruction using filtered backprojection (FBKP), in order to ensure a pure spatial distribution of spin density in the final image. This step can also be highly sensitive to SNR. These factors very often limit the magnitude of the gradient that can effectively be used in practice, and hence the achievable resolution [14]. Overall, to obtain a high resolution image, it is generally admitted that it is preferable to measure paramagnetic centers present in high concentration, giving a strong signal, and more importantly with a simple and narrow linewidth. Of course this ideal situation is rarely met.

Apart from this conventional spatial imaging (SI) approach, it is also desirable to include the spectral dimension in EPR imaging. In the spectral-spatial imaging modality (SSI), EPR spectra are obtained when a series of magnetic field gradients of different magnitude is used instead of static gradients [13,15]. In biomedical applications, this mode is mainly used for the measurements of pO_2 [16–20] or pH microenvironment [21,22]. SSI has also been used in order to characterize polymers, but surprisingly by a very small number of laboratories. Ohno first demonstrated that the degradation of polypropylene (PP) could be monitored using EPRI because this polymer, when exposed to UV light, generated stable nitroxides free radicals. They originated from hindered amines used as stabilizers. Lucarini et al. carried out detailed studies on PP using 1D EPRI [23–25], Marek et al. extended the work to polystyrene [26], while Schlick and collaborators used both 1D EPRI and 2D SSI to study the degradation of heterophasic system such as poly(acrylonitrile–butadiene–styrene) and propylene–ethylene copolymers [27,28], or very recently to measure diffusion coefficients of nitroxide radicals in propylene–ethylene copolymers [29] (for review on this topic see Refs. [30–32] by Schlick).

In these works, the EPR signal arose from stabilizers exposed to UV light or thermal treatment but not from the polymer itself, as it gave no EPR signal at all. Stabilizers were used as a tracers of the morphology and degradation of the polymer.

In this study, we report the use of EPRI, both in SI mode and in SSI mode, to study the properties of photopolymerizable dimethacrylate-based resin-composites used in routine dental practice to fill dental cavities [33].

The resin-based composites used in dentistry are mainly composed of inorganic fillers (from 50% to 80% w/w), dispersed in an organic matrix made of various dimethacrylate monomers (from 20% to 50% w/w), also containing a photoinitiating system (1% w/w or less) [34]. During the restoration of a tooth, this material is placed in the cavity, shaped, and then photopolymerized in situ using a light-curing device emitting in the blue range of the visible spectrum [35]. The polymerization process is based on the production of free radicals, leading to a chain reaction connecting the dimethacrylate monomers to each other and generating a three-dimensional polymer network [33]. It has been described that after photopolymerization, dental resins contain two types of free radicals which are trapped in the polymer network, namely an allylic radical and a so called propagating radical [36]. They both give an EPR signal with hyperfine splitting and the resulting spectrum is an intense and complex multiline spectrum which remains detectable up to 3 months after polymerization, depending on the storage environment [37,38]. EPR spectroscopy turned out to be very useful to improve the knowledge of dental resins [37–39]. However, the use of EPRI has not yet been investigated to characterize this type of material, possibly because of the unfavorable properties of their spectrum. This was the main goal of the present work.

Moreover, to evaluate the ability of EPRI to detect the effect of clinically relevant parameter changes, two different light irradiances were used to initiate the polymerization.

Two types of resin were also selected: a commercial material containing inorganic fillers and an experimental formulation containing only the organic matrix. The spin density distribution was studied using conventional 2D EPRI. Two dimension spectral-spatial images were also acquired to study the specific spatial distribution of the two types of radicals. The resolution of the images was experimentally assessed through the determination of the Edge Spread Function (ESF). For comparison purposes, a usual parameter used to evaluate the quality of photopolymerization of dental dimethacrylate-based resins, i.e. the degree of conversion (DC), was measured using Raman microspectrometry.

2. Material and methods

2.1. Resins

Two types of resin-based materials were used for this work. The first one was an experimental resin containing no inorganic fillers, and made of an equimolar mixture of bisphenol A glycidyl dimethacrylate (Bis-GMA) (Heraeus Kulzer, Wehrheim, Germany) and triethylene glycol dimethacrylate (TEGDMA) (Aldrich, Belgium), with 0.5% (w/w) of camphorquinone (CQ; Aldrich, Belgium) and 0.5% of N,N-dimethyl-p-aminobenzoic acid ethyl ester (DABE, Aldrich) as photoinitiator system [34].

The second material was the commercially available Tetric EvoCeram A3 (Ivoclar-Vivadent, Schaan, Liechtenstein) containing 70% (w/w) inorganic fillers [34].

In a first series of experiments, resins were cast into cylindrical transparent plastic molds (diameter, 4.5 mm; length 10.0 mm) and photopolymerized with a Bluephase G2 visible light-curing device (Ivoclar-Vivadent, Schaan, Liechtenstein) for 40 s. either in the high irradiance (1200 mW/cm^2) or low irradiance mode (650 mW/cm^2). The irradiance of the light was checked using a curing radiometer (Bluephase meter, Ivoclar Vivadent). The photopolymerization was initiated only at the upper end of the sample to induce a gradient of polymerization along the long axis of the sample.

The four groups of samples, experimental resin-high irradiance (A), experimental resin-low irradiance (B), commercial resin-high irradiance (C) and commercial resin-low irradiance (D), were studied using 2D conventional spatial EPRI, as described in the next section.

In a second set of experiments, resins were cast in a rectangular opaque PTFE (polytetrafluoroethylene) mold ($5 \times 5 \times 10$ mm), in order to simulate more clinically relevant conditions. Polymerization was induced during 20 s., which is a typical irradiation time for clinical use, again either at low (650 mW/cm^2) or high irradiance (1200 mW/cm^2). The samples were imaged in both 2D SI and 2D SSI EPRI (cf. infra).

2.2. Image acquisition

Images of the first series of samples cast in transparent molds were acquired in 2D spatial EPRI mode. 2D spatial imaging measures the spin density within the sample and reflects the concentration of free radicals.

The second series of samples, cast in opaque PTFE molds, was imaged both in the spatial imaging mode and in the spectral spatial mode. Spectral images allow to acquire the EPR spectrum for each pixel and consequently to determine parameters such as the linewidth or the intensity of each line throughout the sample.

2.2.1. Spatial imaging

The SI EPR images were acquired at room temperature using an EPR Elexsys E540 System (Bruker, Rheinstatten, Germany) with three orthogonal water-cooled cylindrical gradient coils. The samples were positioned in the center of an X-Band EPR Super High Q cavity cylindrical resonator (ER 4122SHQE, 10 mm diameter) operating at ~9.5 GHz.

The main parameters used for 2D spatial imaging were as follows: microwave power level, 0.5 mW; modulation frequency, 100 kHz; modulation amplitude, 0.1 mT; sweep width, 21.0 mT; time constant, 20.48 ms; conversion time, 10.24 ms. The field of view was 20.0 mm, pixel size 0.5 mm, magnetic field gradient 463 mT m^{-1}. The acquisition time was 4 min. Images were acquired exactly 1 h after the end of the polymerization. The polymerization process lasted for a few seconds and was completely ended when the acquisitions were started.

2D images were reconstructed on a 128 × 128 matrix by filtered backprojection using a Shepp-Logan filter [40]. The raw image is a convolution of the lineshape in the absence of the gradient with the spatial distribution of the paramagnetic species. In order to obtain an image which reflects the true spin density distribution, projections must be deconvoluted. Consequently, before reconstruction, each projection was deconvoluted using fast Fourier transformation with the measured zero-gradient spectrum in order to improve image resolution. To reduce noise amplification and avoid possible division by zero at high frequencies, a low pass filter was used. The deconvolution parameters, including the maximum cut-off frequency and the width of the window in the Fourier space, were set up after viewing the shape of all projections.

Spectral deconvolution and filtered backprojection were performed using the Xepr software package (Bruker).

For each group of samples, a region of interest was drawn by the operator, corresponding to a threshold of 66% of the maximum intensity. The length of this region was measured using the graphical tools of the Xepr software. Statistical analysis was conducted by using JMP 8.0. The influence of the group was assessed by using ANOVA and differences between groups were tested by the Tukey–Kramer honestly significant difference (Tukey HSD).

2.2.2. Spectral spatial imaging

Two dimension spectral spatial images were acquired at room temperature with the following specific spectral parameters: sweep width 36.5 mT, spectral width 20.0 mT, spectral resolution 0.4 mT/p; pixel size 0.3 mm. The field of view was reduced to 15.0 mm. Other parameters were the same as for conventional 2D images. Images were reconstructed on a 128 × 128 matrix grid, without prior deconvolution. Acquisition time was 40 min. Images were acquired 1 h after the end of the polymerization process.

The density of specific trapped radicals in the resin were determined by measuring the height of the fifth (allylic) and fourth (propagating) peaks of the 9-line spectrum, with the Image Viewer software from Bruker. These peaks are least influenced by the signal of the other radical type, as described in previous work [37,38].

2.3. Resolution

The resolution was experimentally determined using a rectangular phantom made from the experimental resin, without fillers, which produced the strongest signal. The resin was placed in a PTFE mold (Lenght 25 mm, Width 5 mm, Thickness 2 mm) and photopolymerized during 40 s. on both sides using a light oven (Dentalcolor XS, Kulzer, Wehrheim, Germany) to ensure a homogeneous polymerization. Spatial 2D EPR image was acquired on the same EPR imager as in the previous experiments, using the same parameters, with the exception of the field of view increased up to 30.0 mm. Sweep width was 30.0 mT, pixel size 0.3 mm. Three scans were acquired for each projection.

The spatial resolution was evaluated in terms of the Edge Spread Function (ESF). ESF was determined following a procedure modified from the classical method used in MRI [41] and from the work of Halpern's group [42–44], as previously published by our laboratory [45,46]. The signal along a line perpendicular to the edge of the phantom was extracted from the image and the derivative was calculated. The derivative curve was computed from the edge-curve without smoothing of the curve, which was then fitted by a Gaussian function:

$$f(x) = \frac{1}{\sigma\sqrt{2\pi}} e^{-\frac{(x-\mu)^2}{2\sigma^2}} \quad (2)$$

From the computed σ values, the Full Width at Half Maximum (FWHM) of the Gaussian curve was calculated from the following equation:

$$\mathrm{FWHM} = 2 \cdot \sigma\sqrt{2 \cdot \ln 2} \quad (3)$$

All calculations and fitting were carried out using Prism 4 from GraphPad Software Inc, La Jolla (CA) USA.

The theoretical spatial resolution, which represents the shortest distance (d) between two points that can be resolved in an EPR image was calculated as follows:

$$d = LW/G \quad (4)$$

where LW (mT) is the linewidth of an EPR signal, and G (mT/m) is the magnitude of the magnetic field gradient.

2.4. RAMAN microspectrometry

The DC was measured using a Raman Spectrometer [47] (DXR Raman Microscope, Thermo Scientific, Madison, WI, USA) on the upper surface and then every half-millimeter on the side of the sample (n = 3) [34]. The samples were excited at 780 nm by a frequency-stabilized single mode diode laser through a microscope objective (50×) and spectra were obtained in the region 1600 cm^{-1}, with the following conditions: microhole, 50; irradiation time, 60 s; number of accumulations, 5; grating 400 lines/mm. The DC was then calculated as the percentage of vinyl functions converted to aliphatic functions based on the decrease in the C=C bond peak at 1640 cm^{-1} compared to the uncured sample; the aromatic C=C peak at 1610 cm^{-1} was used as the internal standard.

3. Results and discussion

3.1. Spatial imaging

Fig. 1 shows the distribution of the trapped radicals within a small sample of either unfilled resin, or commercial resin containing inorganic fillers, both of them polymerized using a transparent mold. The intensity depicted is the integral of signals due to both the allylic and the propagating radicals. For the experimental resin (unfilled), it can be observed that the maximum intensity, hence the concentration of trapped radicals, was much higher when the resin was photopolymerized using a high curing light irradiance (Fig. 1B) than when using low curing light irradiance (Fig. 1C). For a constant irradiation time (here 40 s.), the use of a higher irradiance initiates the creation of more free radicals during the

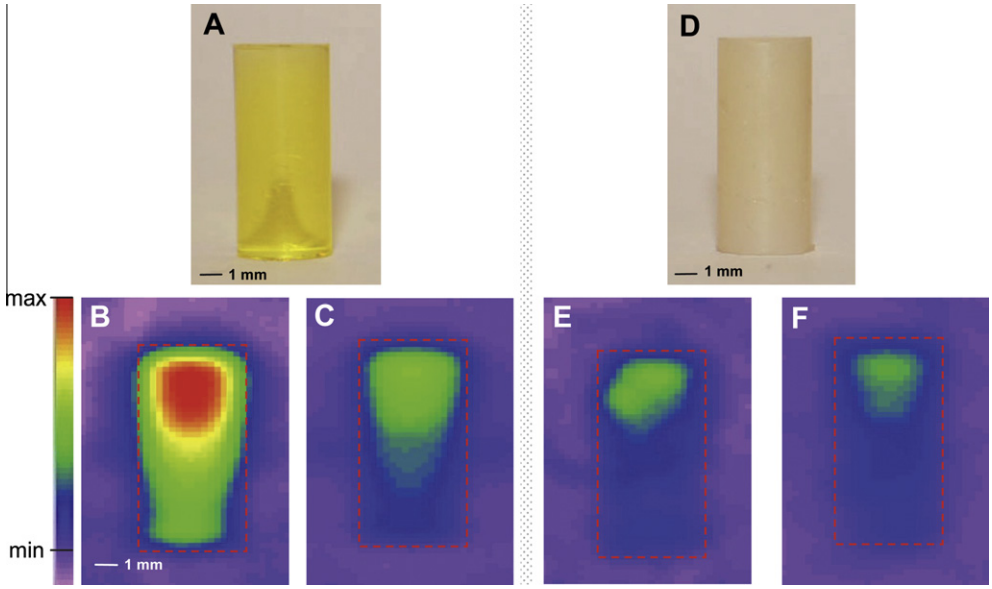

Fig. 1. Influence of the irradiance power mode used for polymerization on the signal intensity in experimental and commercial resins. Experimental resin (A) and the corresponding EPR images, when polymerized with high (B) or low (C) irradiance light-curing modes. Commercial resin (D) and the corresponding EPR images, when polymerized with high (E) or low (F) irradiance light-curing modes. Images intensities are normalized to the maximum intensity of image B. Dashed rectangles show the limits of the samples. Experimental (unfilled) and commercial (filled) resins, were polymerized using a transparent mold.

photopolymerization process, leading to a larger amount of trapped radicals in the vitrified product [38]. Now, considering the commercial composites containing around 70% (w/w) of inorganic filler, a much lower density of trapped radicals was observed (Fig. 1E and F). This is quite logical as only the organic phase of the composite, which contains the free radical species, contributes to the EPR signal, and not the inorganic fillers.

Overall, it could also be noted that the relative radical density decreased within the object as the distance from the illumination point (located at the upper surface of the sample; dist. = 0 mm) increased. In other words a gradient of radical concentration was noted from the upper to the lower surface of the sample. The concentration of trapped radicals remained higher on a longer distance for experimental resins than for commercial composites (Fig. 2). Experimental resins are almost transparent, allowing the propagation of light on a longer distance. On the contrary, commercial resins are heavily charged with inorganic fillers (silica and glass particles) which scatter the light and therefore reduce drastically its transmission in depth. Consequently, the polymerization of the samples is incomplete in the deeper layers, especially in highly filled commercial composites. This problem is well-known in dental practice. It is therefore recommended to fill the cavities by successive incremental layers of maximum 2 mm thickness in order to ensure maximum hardness of the material [34].

Projections were deconvoluted with the zero gradient spectrum before FBKP reconstruction, and no major artifacts were observed on the reconstructed images, despite the complex multiline spectrum showed by this type of material.

Images were acquired exactly 1 h after the start of the polymerization process. As the acquisition time was short (4 min), the variation of the intensity during the acquisition could be expected to be relatively little. The acquisition time for SSI was longer (40 min.). During this period, the intensity of the allylic peak decreased by 3%, and the propagating one by 6%, as already shown by Leprince et al. [37,38]. Because this variation was small, images were not corrected for this decay. In addition, images acquired 24 h

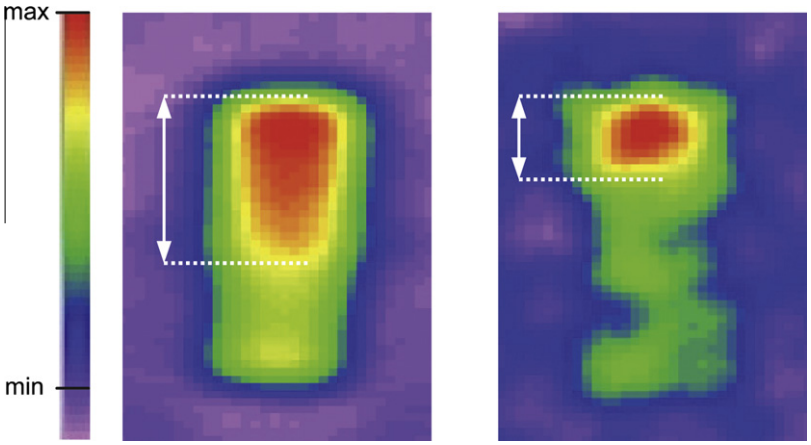

Fig. 2. Distribution of trapped radicals according to the type of resin and the light irradiance. 2D spatial EPR images reveal the density of trapped radicals in an experimental (unfilled) resin irradiated with the high irradiance mode (left) and in a commercial (filled) resin irradiated in the low irradiance mode (right), using a transparent mold. Arrows and dotted lines delimit the vertical limits of a region corresponding to 66% of the maximum intensity.

after polymerization, when the variation of intensity was almost zero, showed a lower intensity but a similar pattern compared to the 1 h images (data not shown).

Leprince et al. also described an effect of the temperature on the kinetics of the signal intensity. However, temperature changes below the Tg (generally around 45–50 °C) have very little impact on the radical decrease. Although our images were acquired without thermostatization, the influence of this parameter on our results is expected to be very low and in our opinion can be neglected.

Apart from the type of resin used, the influence of the light irradiance could also be observed (Fig. 1 – Table 1). For both experimental resin and commercial composite, the area of maximum intensity was much larger in sample photopolymerized at high irradiance than at low irradiance (Fig. 1B vs 1C, Fig. 1E vs 1F – Table 1 – ANOVA analysis: $F_{3,28} = 22.2$; $p < 0.0001$). Experimental resin polymerized using the high irradiance mode showed that the intensity of the signal remained above the selected threshold (66%) up to 4.5 ± 0.2 mm from the illumination point, which is significantly different from the experimental-low irradiance (group B, Tukey HSD $p = 0.052$), the commercial-high irradiance (group C, $p < 0.001$), or the commercial-low irradiance group (group D, $p < 0.001$). The last group, which was the commercial resin-low irradiance group (group D), showed a significantly lower value range of 2.3 ± 0.2 mm ($p = 0.003$).

This first series of experiments was carried out using samples polymerized 40 s. in a transparent mold, acting as a light guide. The same experiment was repeated with a polymerization time of 20 s. and using an opaque mold in order to simulate more clinically relevant conditions.

For the same light irradiance, the maximum intensity is reduced by a factor ~20 between the experimental resin and the commercial one (Fig. 3B and E). A very low signal is recorded in the distal part of the sample (Fig. 3B and C) or even no signal at all for the commercial resin (Fig. 3E and F), as compared to the situation in the first series. In this configuration, the mold did not act as a light guide as it did in the first series (Fig. 1), so that no light was transmitted along the side of the mold, but only through the resin material. Traveling across the material from the illumination point, the light is progressively absorbed (by photoinitiators and pigments) and scattered (by inorganic fillers) so that not enough light reaches the deeper material to initiate free radicals. This is in agreement with the observation that the end of the sample (commercial resin) remained soft (see the difference of texture in the lower part of the sample on Fig. 3D). For the commercial resin, the signal was the most intense in the upper 2 mm layer, which corresponds to the maximum thickness generally recommended for each successive composite layer in clinical practice.

In summary, 2D spatial EPRI was able to distinguish the distribution of radicals in dental resins, based on the type of resin used, as well as on the light irradiance used to initiate the photopolymerization.

3.2. Spectral-spatial imaging

The spectral spatial mode of EPRI allowed to record the complete EPR spectrum for each pixel of the image (Figs. 4 and 8). It is also possible to measure the linewidth and the intensity of selected lines, here corresponding to the allylic or propagating radicals. We did not observe any variation of the linewidth throughout the sample, whatever the series tested, neither for the allylic peaks nor the propagating peaks. Consequently, the measure of the peak height on the first derivative of the spectrum is a reliable measurement of the spin density, and hence of the radical concentration for each type of radical. It must be noted that the intensity of the central peak is the sum of the intensities of both species. Nevertheless, the intensity of the propagating species (4th peak) was low compared to the intensity of the allylic central peak so that its contribution was not expected to be more that 10% of the measured intensity.

Table 1
Size of the region of interest corresponding to an intensity of 66%, according to the type of resin and the irradiance of the lamp used for polymerization. Results are mean ± SE ($n = 3$).

	Type of resin	
Irradiance intensity	Experimental	Commercial
High (1200 mW/cm^2)	4.5 ± 0.2 mm	3.0 ± 0.2 mm
Low (600 mW/cm^2)	3.6 ± 0.2 mm	2.3 ± 0.2 mm

Whereas the linewidth remained constant, a variation of the intensity of the peaks with the distance was observed both for the allylic radical and the propagating radical (Fig. 5). In the experimental resin, the maximum intensity of the allylic peak was observed over a two millimeter-long region from the illumination point, followed by a slow and regular decrease (Fig. 5, left). A similar situation was observed for the commercial composite, but it decreased more rapidly, with almost no signal after 7 mm, most probably because the composite is less transparent to light than the unfilled resin, as already mentioned. As observed in SI, experimental resin illuminated in the high irradiance mode showed the most intense signal, especially in depth, whereas the commercial resin irradiated at low irradiance showed the weakest signal.

The propagating peak showed a different evolution. The intensity was also maximum in a two millimeter region from the illumination point, but a much more rapid decrease was then observed in the deeper level, with a signal decreasing to a very low intensity, sometimes almost undetectable. As pointed out above, there was a contribution of this signal in the allylic curve, because the two signal were superimposed, but this signal was low and decreased rapidly to almost zero so that its global influence could be considered as marginal.

Previous studies have described a major difference in reactivity between these two species: allylic radicals are very stable because of a resonance phenomenon, whereas propagating radicals are very reactive [37,38]. Hence, an insufficient polymerization in the depth of the material can lead to a local network mobility that is sufficient for propagating radicals to terminate, but not for the allylic ones.

3.3. RAMAN microspectrometry

As mentioned earlier, resin-based composite materials are often characterized by using Raman spectrometry. For comparison purposes with this classic method, we measured the degree of conversion (DC) for each type of resin and for both light irradiances (See Fig. 6). For the experimental resin, the DC remained almost constant throughout the depth of the sample, which tends to show that the polymerization quality is homogeneous throughout the sample. On the contrary, for the commercial resin, DC rapidly dropped to reach almost zero in the 8 mm region, when the lamp is used in the low irradiance mode. In general, it is believed that DC is a good measurement of the quality of cure of resin-based materials. However, a recent paper demonstrated that DC is insufficient to evaluate the quality of cure in depth of these materials [48]. According to this work, it is difficult to determine which DC corresponds to "adequate" polymerization.

The present results suggest that EPRI could be a useful complementary method to further characterize this type of material.

3.4. Resolution

Finally, the experimental resolution of the 2D SI images was estimated by the Edge Spread Function (Fig. 7). The σ parameter

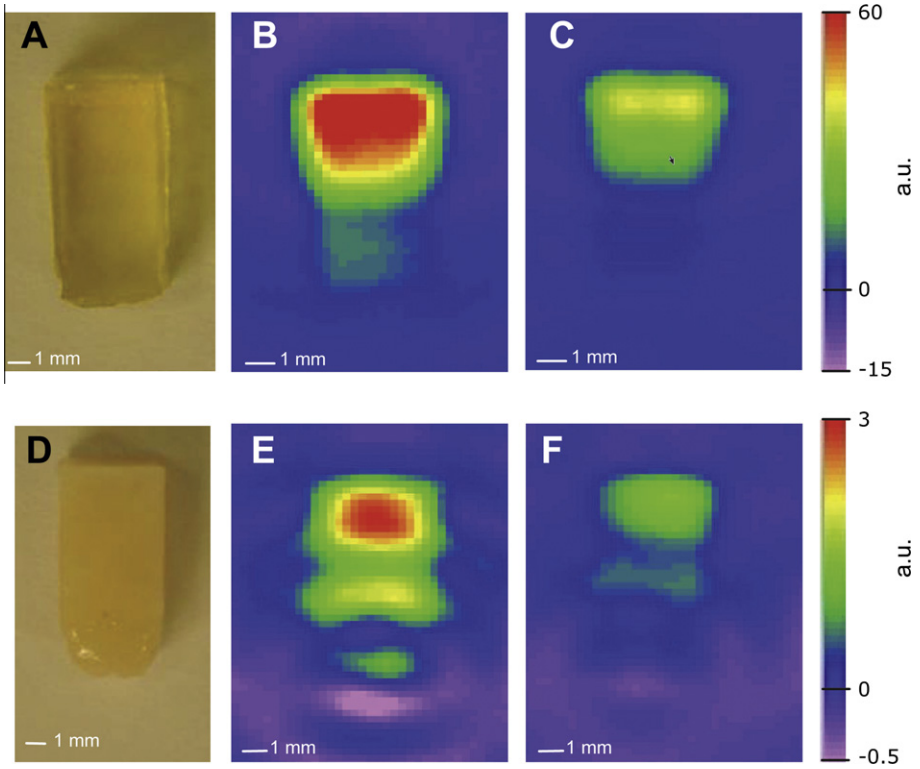

Fig. 3. Relative densities of free radicals in resins polymerized in an opaque mold. Polymerization was induced on the upper side of the sample. Experimental (unfilled) resin (A) ligh-cured for 20 s. in the high (B) or low (C) irradiance mode. Commercial resin (unfilled) (D) light-cured for 20 s. in the high (E) or low (F) irradiance mode. Note the difference of scale between fig B–C and E–F.

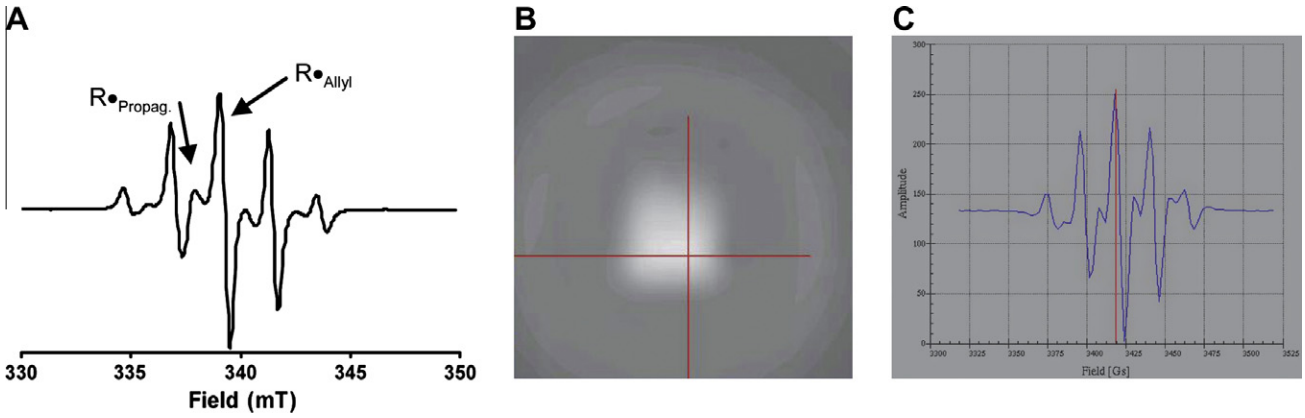

Fig. 4. 2D spectral spatial EPRI. EPR spectrum of an experimental resin showing a complex pattern with hyperfine splitting (A). High peaks are mainly due to the allylic radical, and small peaks are due to the propagating radicals. In 2D spectral spatial imaging mode, each voxel of the image (B) contains the corresponding spectrum on which standard parameters such as linewidth or lineheight can be measured (C).

calculated from the Gaussian fit of the ESF curve was 0.40 (95% CI: 0.37–0.42) (Eq. (2)). The resolution expressed as FWHM was 0.94 mm (95% CI: 0.88–0.99 mm) (Eq. (3)).

Theoretical resolution is governed by the linewidth of the spectrum and the magnitude of the gradient used according to Eq. (4). As the spectrum is a complex multiline one, the mean linewidth can be estimated in different ways. A first possibility is to measure the mean value of the central line, assuming that it represents the main contribution in the image. The mean linewidth of the central line was 0.5 mT with a corresponding resolution of 1.08 mm, for a gradient strength of 466.0 mT m^{-1}. Another possibility is to deconvolute the spectrum with itself, using the parameters selected for the reconstruction of the image in order to simulate the linewidth used for the reconstruction. The linewidth measured with this procedure was also 0.5 mT and the resolution was 1.08 mm. When the signal to noise was very high, the deconvolution process could be pushed up and it was possible to reach a LW of 0.06 mT and a theoretical resolution of 0.13 mm. Nevertheless this was not possible on standard samples. The approach used in this work to experimentally assess the resolution is a holistic approach which gives a global resolution, affected by several factors. Apart from instrumental limitations, the resolution is also influenced by the quality of the phantom and more specifically by the material itself and the conditions of polymerization. Oxygen is a well known inhibitor of polymerization. Because it diffuses very slowly in the material, it is likely that it exerts its effect mainly on the surface level and on the

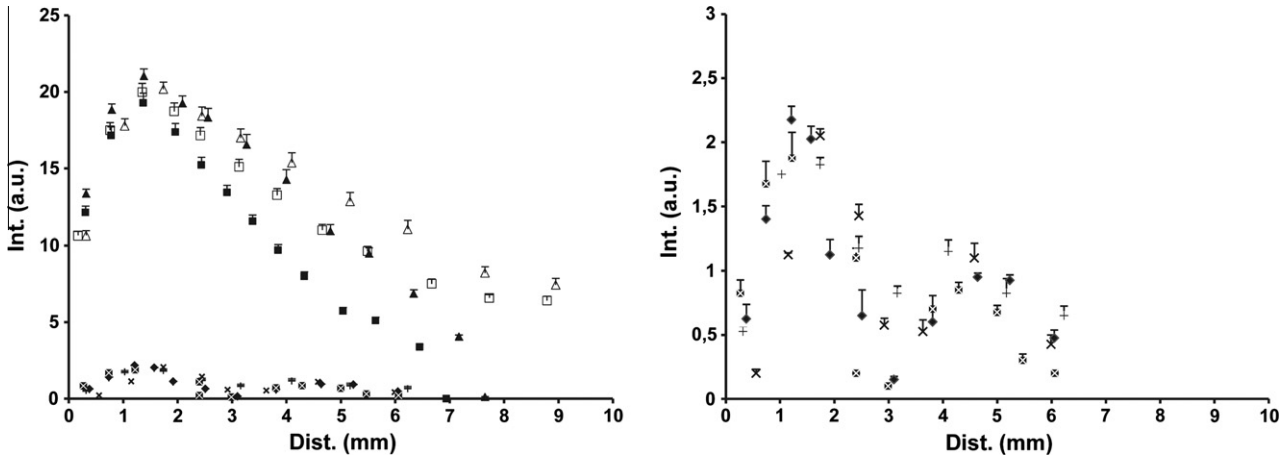

Fig. 5. Evolution of the intensities of allylic radical and propagating radical peaks (2D SSI) with the distance from the illumination point, which corresponds to dist. = 0 mm. Results are means ± SE (n = 4). Allylic peak (left pannel): experimental resin high (△) or low irradiance (□) vs commercial resin high (▲) or low irradiance (■) mode. The low intensity curves (propagating peak) are plotted with appropriate scale on the right pannel. Propagating peak (right pannel): experimental resin high irradiance (+) or low irradiance (**X**) vs commercial resin high (♦) or low irradiance (⊠) mode.

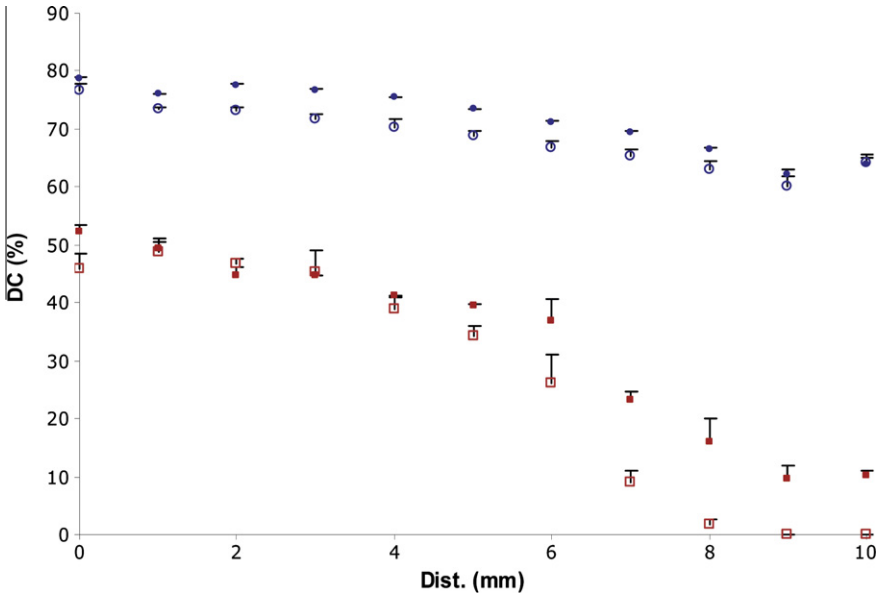

Fig. 6. Evolution of the Degree of Conversion (DC) from the illumination point (=0 mm), measured with Raman spectrometry. Commercial resin (filled) light-cured with high (■) or low irradiance mode (□). Experimental resin (unfilled) light-cured with high (●) or low irradiance mode (O). Each point is the mean ± SE (n = 3).

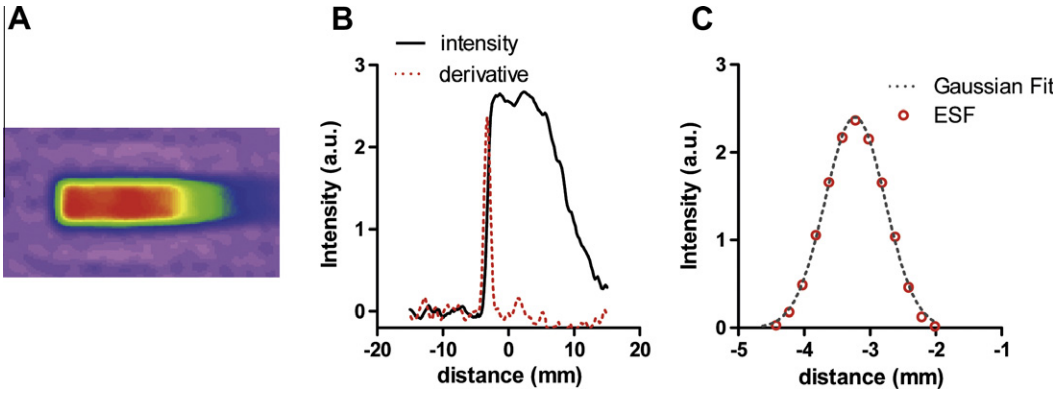

Fig. 7. Determination of the Edge Spread Function (ESF) and computation of the experimental resolution. The 2D image of a rectangular phantom was acquired in standard 2D mode (A), and a profile of the intensity along the long axis was extracted and the first derivative of the curve was computed (B). The first derivative was fitted with a Gaussian function and the σ parameter determined from this fit (C).

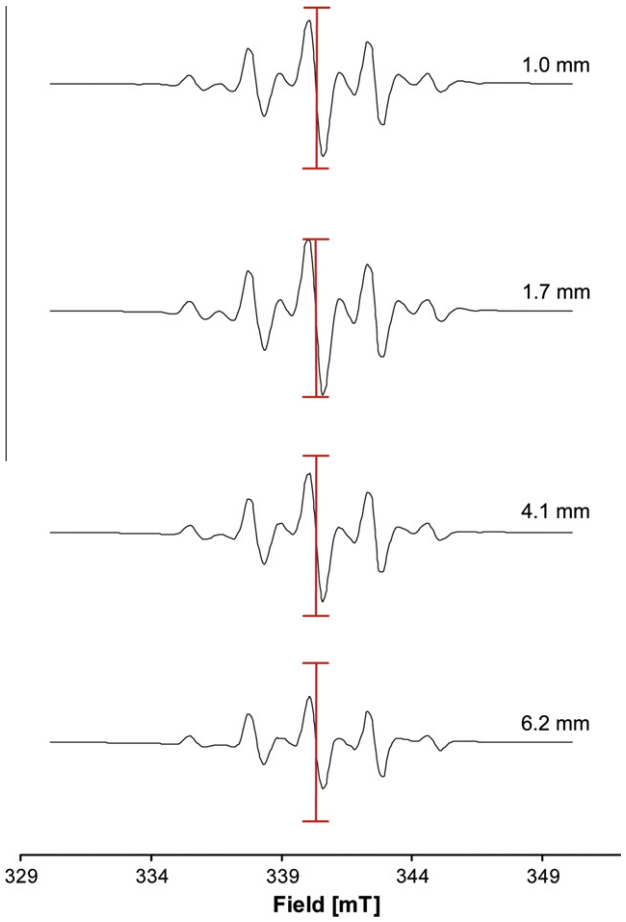

Fig. 8. Evolution of the EPR spectrum from the illumination point. Spectra were obtained in spectral-spatial imaging at different coordinates along the vertical axis of the object. The distance mentioned next to each spectrum is the distance measured from the top of the sample. The red scale was set to the maximum intensity of the central peak measured at 1.7 mm from the origin.

edges of the phantom. As the latter was relatively thin, oxygen could be responsible of a lower degree of polymerization, and hence a lower signal on the edges. Apart from the instrumental factors, this could also partially explain why a gradient of signal intensity is observed from the edges. This phenomenon degrades the resolution but is inherent to the material used, and must also be taken into account when evaluating the resolution.

The resolution achieved in this study was sufficient for our purpose, but would be a limiting factor for studying samples of smaller size, which would be more interesting to mimic samples used in routine dental practice. The magnitude of the gradient on our system was limited to 500.0 mT m^{-1} but it is likely that the resolution could be markedly improved using a higher gradient of magnetic field, available on more recent imager. A higher gradient would induce a strong widening of the signal, and consequently lower the SNR. Nevertheless the SNR observed under our conditions was extremely good, so that it is not likely that this ratio would suffer from the distortion imposed by a higher value of gradient. Another possibility for increasing the resolution would be to improve the reconstruction process by using optimized algorithms [49].

4. Conclusion

Photopolymerizable dimethacrylate-based dental resins, which are widely used in the current routine dental practice, show a very strong EPR signal, but also a quite complex spectrum due to hyperfine splitting and to the presence of two radical species, a characteristic which is a priori not favorable for EPR imaging. We have demonstrated that, despite this complex spectrum, it is possible to acquire images of small samples made of experimental or commercial resins, using the standard algorithm available in commercial package. The spectrum complexity requires the application of a deconvolution step prior to reconstruction, a process which is usually very sensitive to the SNR. In our hands, it gave images without noticeable artifact, probably because the intensity of the signal is remarkably intense. The distribution of the radicals as assessed by EPRI correlates well with the type of resin used, or the irradiance of the light used. Moreover, spectral spatial imaging was successfully performed. It allows to study the evolution of each type of radical in the resin. We have shown a different distribution between the two radicals, which correlates with the variation of the physical state of the resin. This implies a different mechanism of termination for each radical.

The experimental resolution of the image, expressed as FWHM, is currently limited by the magnitude of the gradient of magnetic field, but could be easily increased with more recent imager, disposing of higher gradients.

Overall, we have demonstrated that EPRI is a valuable tool to study the properties of biomaterial such as dimethacrylate-based dental resins, and should be considered along with other methods such as Raman spectroscopy and other techniques used so far to characterize this type of material.

References

[1] G.R. Eaton, S.S. Eaton, Kev M. Salikhov, Foundations of Modern EPR, World Scientific Publishing, Singapore, 1998.
[2] S.S. Eaton, G.R. Eaton, L.J. Berliner, Biomedical EPR part A: free radicals, metals, medicine, and physiology, in: Biomedical EPR, Kluwer Academic Plenum, New York, 2005, p. 522.
[3] S.S. Eaton, G.R. Eaton, EPR imaging, Journal of Magnetic Resonance 59 (1984) (1969) 474–477.
[4] L.J. Berliner, In vivo EPR (ESR): Theory and Application, Kluwer Academic/Plenum Publishers, 2003.
[5] W. Karthe, E. Wehrsdorfer, The measurement of inhomogeneous distributions of paramagnetic centers by means of EPR, Journal of Magnetic Resonance 33 (1979) 107–111.
[6] M.J.R. Hoch, Electron spin resonance imaging of paramagnetic centers in solids, Journal of Physics C: Solid State Physics 14 (1981) 5659–5666.
[7] M.J.R. Hoch, A.R. Day, Imaging of paramagnetic centers in diamond, Solid State Communications 30 (1979) 211–213.
[8] J.L. Berliner, H. Fujii, Magnetic resonance imaging of biological specimens by electron paramagnetic resonance of nitroxide spin labels, Science 227 (1985) 517–519 (New York, NY).
[9] L.J. Berliner, H. Fujii, X.M. Wan, S.J. Lukiewicz, Feasibility study of imaging a living murine tumor by electron paramagnetic resonance, Magnetic Resonance in Medicine 4 (1987) 380–384.
[10] H. Fujii, L.J. Berliner, One- and two-dimensional EPR imaging studies on phantoms and plant specimens, Magnetic Resonance in Medicine 2 (1985) 275–282.
[11] G.R. Eaton, S.S. Eaton, K. Ohno, EPR Imaging and In vivo EPR, CRC Press, 1991.
[12] S. Subramanian, K. Matsumoto, J.B. Mitchell, M.C. Krishna, Radio frequency continuous-wave and time-domain EPR imaging and Overhauser-enhanced magnetic resonance imaging of small animals: instrumental developments and comparison of relative merits for functional imaging, NMR in Biomedicine 17 (2004) 263–294.
[13] M. Maltempo, G.R. Eaton, S.S. Eaton, Spectral spatial imaging, in: G.R. Eaton, S.S. Eaton, K. Ohno (Eds.), EPR Imaging and In vivo EPR, CRC Press, Boca Raton, 1991.
[14] R.K. Woods, W.B. Hyslop, R.B. Maar, P.C. Lauterbur, Image reconstruction, in: G.R. Eaton, S.S. Eaton, K. Ohno (Eds.), EPR Imaging and In vivo EPR, CRC Press, Boca Raton, 1991, pp. 91–117.
[15] G.R. Eaton, S.S. Eaton, M.M. Maltempo, Three approaches to spectral-spatial EPR imaging, Applied Radiation and Isotopes 40 (1989) 1227–1231.
[16] R. Ahmad, P. Kuppusamy, Theory, instrumentation, and applications of electron paramagnetic resonance oximetry, Chemical Reviews 110 (2010) 3212–3236.
[17] B. Gallez, C. Baudelet, B.F. Jordan, Assessment of tumor oxygenation by electron paramagnetic resonance: principles and applications, NMR in Biomedicine 17 (2004) 240–262.
[18] B. Williams, H. Halpern, In vivo EPR imaging biomedical EPR, Part A: free radicals, metals, medicine, and physiology, in: S. Eaton, G. Eaton, L. Berliner (Eds.), Springer, US, 2005, pp. 283–319.

[19] H.J. Halpern, C. Yu, M. Peric, E. Barth, D.J. Grdina, B.A. Teicher, Oxymetry deep in tissues with low-frequency electron paramagnetic resonance, Proceedings of the National Academy of Sciences 91 (1994) 13047–13051.
[20] B. Epel, S.V. Sundramoorthy, E.D. Barth, C. Mailer, H.J. Halpern, Comparison of 250 MHz electron spin echo and continuous wave oxygen EPR imaging methods for in vivo applications, Medical Physics 38 (2011) 2045–2052.
[21] F. Eisenächer, A. Schädlich, K. Mäder, Monitoring of internal pH gradients within multi-layer tablets by optical methods and EPR imaging, International Journal of Pharmaceutics 417 (2011) 204–215.
[22] S. Kempe, H. Metz, K. Mäder, Application of electron paramagnetic resonance (EPR) spectroscopy and imaging in drug delivery research – chances and challenges, European Journal of Pharmaceutics and Biopharmaceutics 74 (2010) 55–66.
[23] M. Lucarini, G. Pedulli, V. Borzatta, N. Lelli, X-band EPR imaging of polymers irradiated with UV light, Research on Chemical Intermediates 22 (1996) 581–591.
[24] P. Franchi, M. Lucarini, G.F. Pedulli, M. Bonora, M. Vitali, Time evolution of the concentration profiles of HALS stabilizers and of the corresponding oxidation forms across poly(propylene) plaques irradiated with UV-visible light, Macromolecular Chemistry and Physics 202 (2001) 1246–1256.
[25] M. Lucarini, G.F. Pedulli, Use of EPR to image nitroxyl radicals in hals stabilized polymers, Die Angewandte Makromolekulare Chemie 252 (1997) 179–193.
[26] A. Marek, L. Kaprálková, P. Schmidt, J. Pfleger, J. Humlíček, J. Pospíšil, J. Pilař, Spatial resolution of degradation in stabilized polystyrene and polypropylene plaques exposed to accelerated photodegradation or heat aging, Polymer Degradation and Stability 91 (2006) 444–458.
[27] K. Kruczala, M.V. Motyakin, S. Schlick, ID and 2D electron spin resonance imaging (ESRI) of nitroxide radicals in stabilized poly(acrylonitrile–butadiene–styrene) (ABS): UV vs thermal degradation, Journal of Physical Chemistry B 104 (2000) 3387–3392.
[28] M.V. Motyakin, J.L. Gerlock, S. Schlick, Electron spin resonance imaging of degradation and stabilization processes: behavior of a hindered amine stabilizer in UV-exposed poly(acrylonitrile–butadiene–styrene) polymers, Macromolecules 32 (1999) 5463–5467.
[29] K. Kruczala, S. Schlick, Measuring diffusion coefficients of nitroxide radicals in heterophasic propylene–ethylene copolymers by electron spin resonance imaging, Macromolecules 44 (2011) 325–333.
[30] S. Schlick, K. Kruczala, Spatially resolved degradation in heterophasic polymers from 1D and 2D spectral-spatial ESR imaging experiments, in: Advanced ESR Methods in Polymer Research, John Wiley & Sons, Inc., 2006, pp. 229–254.
[31] S. Schlick, M.V. Motyakin, ESR imaging beyond phantoms: application to polymer degradation, in: Electron Paramagnetic Resonance, The Royal Society of Chemistry, 2007, pp. 1–28 (Chapter 1).
[32] S. Schlick, G. Jeschke, Electron spin resonance, in: Characterization and Analysis of Polymers, Wiley, Hoboken, 2008, pp. 895–932.
[33] N.B. Cramer, J.W. Stansbury, C.N. Bowman, Recent advances and developments in composite dental restorative materials, Journal of Dental Research 90 (2011) 402–416.
[34] J. Leprince, W.M. Palin, T. Mullier, J. Devaux, J. Vreven, G. Leloup, Investigating filler morphology and mechanical properties of new low-shrinkage resin composite types, Journal of Oral Rehabilitation 37 (2010) 364–376.
[35] J. Leprince, J. Devaux, T. Mullier, J. Vreven, G. Leloup, Pulpal-temperature rise and polymerization efficiency of LED curing lights, Operative Dentistry 35 (2010) 220–230.
[36] D. Truffier-Boutry, X.A. Gallez, S. Demoustier-Champagne, J. Devaux, M. Mestdagh, B. Champagne, G. Leloup, Identification of free radicals trapped in solid methacrylated resins, Journal of Polymer Science Part A: Polymer Chemistry 41 (2003) 1691–1699.
[37] J. Leprince, G. Lamblin, D. Truffier-Boutry, S. Demoustier-Champagne, J. Devaux, M. Mestdagh, G. Leloup, Kinetic study of free radicals trapped in dental resins stored in different environments, Acta Biomaterialia 5 (2009) 2518–2524.
[38] J.G. Leprince, G. Lamblin, J. Devaux, M. Dewaele, M. Mestdagh, W.M. Palin, B. Gallez, G. Leloup, Irradiation modes' impact on radical entrapment in photoactive resins, Journal of Dental Research 89 (2010) 1494–1498.
[39] G. Lamblin, J. Leprince, J. Devaux, M. Mestdagh, B. Gallez, G. Leloup, Hydroxyl radical release from dental resins: electron paramagnetic resonance evidence, Acta Biomaterialia 6 (2010) 3193–3198.
[40] F. Natterer, The Mathematics of Computerized Tomography, Wiley, New York, 1986.
[41] D.W. McRobbie, E.A. Moore, M.J. Graves, M.R. Prince, MRI from Picture to Proton, Cambridge University Press, Cambridge, 2003.
[42] K.-H. Ahn, H.J. Halpern, Simulation of 4D spectral-spatial EPR images, Journal of Magnetic Resonance 187 (2007) 1–9.
[43] K.-H. Ahn, H.J. Halpern, Object dependent sweep width reduction with spectral-spatial EPR imaging, Journal of Magnetic Resonance 186 (2007) 105–111.
[44] K.-H. Ahn, H.J. Halpern, Spatially uniform sampling in 4-D EPR spectral-spatial imaging, Journal of Magnetic Resonance 185 (2007) 152–158.
[45] P. Leveque, Q. Godechal, A. Bol, F. Trompier, B. Gallez, X-band EPR imaging as a tool for gradient dose reconstruction in irradiated bones, Medical Physics 36 (2009) 4223–4229.
[46] E.S. Vanea, P. Leveque, F. Abboud, A. Bol, J.M. Denis, N. Kolbun, S. Vynckier, B. Gallez, Evaluation of the dose distribution gradient in the close vicinity of brachytherapy seeds using electron paramagnetic resonance imaging, Magnetic Resonance in Medicine 61 (2009) 1225–1231.
[47] C. Pianelli, J. Devaux, S. Bebelman, G. Leloup, The micro-Raman spectroscopy, a useful tool to determine the degree of conversion of light-activated composite resins, Journal of Biomedical Materials Research 48 (1999) 675–681.
[48] J.G. Leprince, M. Hadis, A.C. Shortall, J.L. Ferracane, J. Devaux, G. Leloup, W.M. Palin, Photoinitiator type and applicability of exposure reciprocity law in filled and unfilled photoactive resins, Dental Materials 27 (2011) 157–164.
[49] H. Hirata, M. Wakana, H. Susaki, Feasibility study of superresolution continuous-wave electron paramagnetic resonance imaging, Applied Physics Letters 88 (2006) (254103/254101–254103/254103).